Simulation and improvement performance of PN (BGaAs/GaAs) and PIN (GaAs/BGaAs/GaAs) junction solar cells

D. Slimi [a], R. Hamila [a], F. Saidi [a,b,*], A. Helali [a], M. Madani [c], M. H. Dhaou [d], D. Ilkay [e]

[a] *Laboratory of micro-optoelectronics and nanostructures (LR99ES29), University of Monastir, Faculty of Sciences Monastir, Environment Avenue5019 Monastir, Tunisia*

[b] *Institut Supérieur des Sciences Appliqués et Technologie de Sousse, Université de Sousse, Tunisia*

[c] *Laboratory for the Development of Renewable Energies and their Applications in Saharan areas (LDREAS), TAHRI Med University of Bechar, Faculty of Exact Sciences, Algeria*

[d] *Department of physics, College of Science, Qassim University, Saudi Arabia.*

[e] *Department of Nanotechnology Engineering and Nanophotonics Research and Application Center, Sivas Cumhuriyet University, 58140 Sivas, Turkey*

This work presents the development of PN, PIN, and P^+PIN solar cells using GaAs and BGaAs in AM1.5G conditions. The structural modeling and simulation of the device were carried out using Silvaco applications. The efficiency of BGaAs and GaAs materials was examined by varying doping concentration and thickness. The study was designed to optimize the physical properties of PN, PIN, and P^+PIN junction cell structures for high efficiency. First, the doping dosage and layer thickness were optimized to create the best possible design for the cells. Then, the conversion capacity, short-circuit current density, fill factor, and open-circuit voltage of the photovoltaic cells were evaluated. Finally, the optimized devices were compared against existing devices in the literature. While the simulated P^+PIN structure efficiency reached 28.2%, compared to 25.2% for the PIN structure, homojunction GaAs attained an efficiency of around 22.4%, compared to the BGaAs/GaAs heterojunction, which only represents 19.6% efficiency. Each solar cell simulation was run at 300 K with 1 sun of normal solar spectrum AM1.5G light intensity.

(Received June 30, 2025; Accepted September 16, 2025)

Keywords: GaAs, BGaAs, Silvaco, PN, PIN, Optical properties, Solar cell

1. Introduction

To meet increasing global energy demands, solar energy has emerged as one of the most promising renewable sources. A photovoltaic cell is a frequently employed device for collecting limitless, free electricity from the sun. Following the first basic single-junction solar cells, thin-film and multijunction photovoltaic panels were created for use in space applications [1]. In fact, direct band gap materials indicate how highly functional single- or multiple-junction photovoltaic cells can be produced by employing an ideal configuration. GaAs solar cells are becoming more and more common due to their bandwidth (1.42 eV), which is close to the typical wavelengths of radio waves [2]. However, the main issue is the material's recombination level, which prevents GaAs solar cells from growing 10% more efficient [3]. This problem has been successfully resolved by integrating boron into GaAs, which may have applications in the optoelectronics sector. Recent studies have focused on quaternary BInGaAs, suggesting that it might be used as an active layer in solar cells and yielding better performance than InGaAsN [4]. This study focuses on building a new solar cell and evaluating how it performs with very efficient III-V materials. Furthermore, an optimization method

* Corresponding author: faouzi.saidi@gmail.com
https://doi.org/10.15251/JOR.2025.215.579

was tested and suggested. The findings achieved with similar solar systems of existing devices are presented and compared. Unlike previous work on the simulation of InGaAs and GaAsN-based [5] solar cells, our study introduces a material level based on the III-V semiconductor BGaAs, which allows for the first time to use BGaAs as an active layer of high-efficiency solar cells. The goal is to achieve a band gap energy of 1.25 eV or 1 eV. This paper starts with a general overview of solar cells, followed by an explanation of the ATLAS simulator and the genetic software used in solar cells. The approach used is then presented, and the entire work is concluded in the last section.

2. Modelling details

The Silvaco TCAD technology is a complete software bundle that enables the modeling and examination of semiconductor devices and processes. One of its key components is ATLAS, a device simulator that utilizes physics to determine the electrical properties of the device's physical layout and bias conditions [6]. In this study, Silvaco ATLAS was employed to run the program in which we modeled III-V semiconductor-based photovoltaic cells in several configurations to maximize the attributes of a solar cell (efficiency, form factor...) [7]. The simulation result was visualized using tonyplot. When creating Silvaco ATLAS code, a few crucial stages must be followed as shown in Fig. 1 [8]. Several factors must be established before a solar cell structure and composition can be generated in ATLAS. Among these factors, one can cite the ATLAS two-dimensional lattice mesh structure in the regions, the materials in each region, the kinds and concentrations of dopants for each material, and the simulated light spectrum specification. The performance of the photovoltaic cells can be estimated by evaluating the voltage during the open circuit and short circuit current after the current density has been removed from the modeling.

Based on the modeling of optoelectronic devices (solar cells) generalized by semiconductor engineering, the fundamental query is: How can solar cells be made more affordable and efficient?

To answer this question, we have selected three different structures to simulate: GaAs (p) /GaAs (n), GaAs (p) /$B_xGa_{(1-x)}$ As (n), and P^+ (GaAs (p) /BGaAs(i) /GaAs (n)).

The goal of this project was to create a photovoltaic device and then enhance its performance. A numerical inquiry was carried out utilizing “Silvaco TCAD” simulation software to assess the impact of physical and geometric features on the performance of the analyzed structures to identify a solar cell's attributes (efficiency, shape...). To evaluate the performance of our structures, a comparative analysis was conducted with other fundamental III-V cells before the conclusion. The ATLAS code was written using TCAD Silvaco software to create the three cells with a gold metal contact on top of the structure. Beneath this gold metal contact, there is a window layer followed by the PN junction for the cells' homo- and heterojunction (the n-type GaAs emitter (or $B_xGa_{(1-x)}$ As) and p-type GaAs base) or the P^+ (PIN junction (GaAs (p)/BGaAs (i)/GaAs(n)).

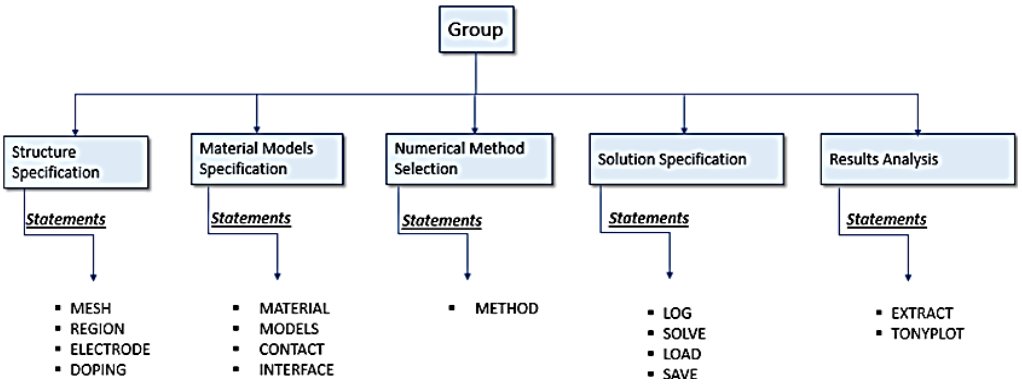

Fig. 1. The major principles related to every Atlas Command Group.

After that, we applied a GaAs buffer layer and a GaAs base, and lastly, a silver contact was attached to the bottom cell. The purpose of the window layer in these solar cells was to capture as much photon from the light source as possible and facilitate the flow of charge without current voltage energy dissipation. The simulation of a PIN structure is very effective in photovoltaic conversion because it decreases the rate of recombination in the heterojunctions surface and volume. Moreover, it increases photo-current by using the electric field to separate the electrons-holes pairs formed in the intrinsic region (This region is undoped) [9]. The structure of P^+PIN junction cell (GaAs/BGaAs/GaAs) is shown in Fig. 2. Therefore, the design of the structure was tested and simulated digitally.

Test 1: GaAs (p) and GaAs (n) homojunction cellular structure without buffer and cap layer

Test 2: GaAs (p) and BGaAs (n) heterojunction cellular structure without buffer and cap layer

Test 3: GaAs/BGaAs/GaAs PIN structure with buffer

Test 4: GaAs/BGaAs/GaAs P^+PIN structure with buffer and cap layer

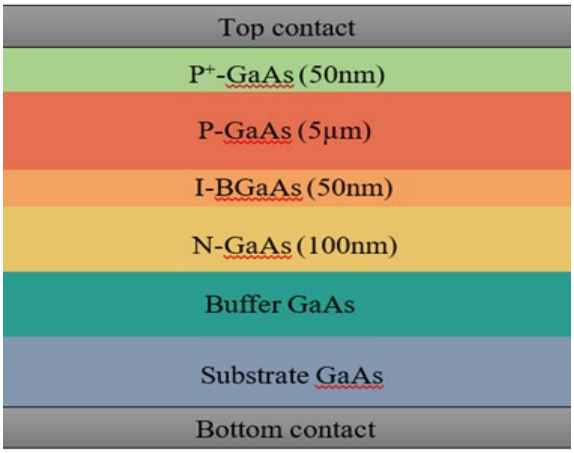

Fig. 2. P+PIN (GaAs/BGaAs/GaAs) solar cell structure.

The data inputs for the suggested solar cells are displayed in Table 1. The literature on Sopra, which is connected to Silvaco, provided the refractive indices of the different materials as well as all the crucial information needed for modeling solar cells [10,11,12]. Each simulation was performed under standard AM1.5G illumination, with an incident power density of 100 mW/cm² and an ambient temperature of 300 K.

Table 1. Principal simulation parameters [13,14,15,16,17,18].

Parameters	**Designation**	**GaAs**	**$B_xGa_{(1-x)}$ As (x=1.46%)**
***Eg** (eV)*	Band gap	1.42	1.39
$\varepsilon_s/\varepsilon_0$	Permittivity	13.1	7.1119
τ_n (S)	Electron lifetime	1×10^{-9}	1×10^{-9}
τ_p (S)	Hole lifetime	2×10^{-8}	1×10^{-9}
χ (eV)	Affinity	4.07	4.18
N_c (cm^{-3})	Electron density of state	4.35×10^{17}	1×10^{17}
N_v (cm^{-3})	Hole density of state	8.16×10^{18}	5.99×10^{18}
MUN ($cm^2 . V^{-1} . s^{-1}$)	e− mobility	8800	100
MUP ($cm^2 . V^{-1} . s^{-1}$)	h+ mobility	400	_

Our Silvaco ATLAS tool simulated ~~a~~ III-V semiconductor-based solar cell. To improve the solar cell, it is crucial to choose the simulation's physical models properly. The main physical models utilized when building any solar cell are Recombination Shockley-Read-Hall (SRH), Auger, Mobility Depend on Concentration and Temperature (ANALYTIC), and Fermi-Dirac Statistics (FERMI). In greater detail, recent studies on B(In)GaAs layers [19] indicated that there is a distribution of states in the band gap due to the difference in size and electronegativity between B and Ga host atoms. The aforementioned distributions result in stress fields and potential fluctuations that enhance phonon and impurity scattering. Consequently, charge carriers undergo a greater frequency of momentum-relaxing collisions, thereby reducing their effective mobility. Furthermore, the introduction of boron atoms, functioning as acceptor dopants, results in the formation of localized states within the band gap. These states facilitate Shockley-Read-Hall recombination, thus increasing non-radiative losses and reducing carrier lifetimes. The ATLAS user manual provides a detailed description of each tool model [20].

The engineering of solar power cells is examined using performance parameters. These components must be incorporated into the method of optimization. The dark (unilluminated) current-voltage characteristic shifted by the short-circuit current I_{sc} describes the current in an illuminated solar cell [21]. This relationship is mathematically described by the Shockley equation:

$$I= I_0 \left[\exp (qV/nkT)-1\right]-I_{ph} \quad (1)$$

Here I corresponds to the resultant current in the solar cell circuit,I_{ph} is photogenerated current, V is the applied voltage,I_0 is diode saturation current (reverse), q denotes the electron charge, n is diode ideality factor, T is temperature in Kelvin, and k is the Boltzmann's constant.

The I_{SC} is defined as the current through the solar cell when V=0:

$$I_{sc} = I_{ph}$$

$$J_{sc} = I_{sc}/A$$

J_{sc} **is** the short-circuit current density (in mA/cm²) from a solar cell when short-circuited while under illumination, A is active area of the photovoltaic cell (cm² or m²).

The open circuit's voltage V_{oc} is another measurement used to characterize a cell that produces electricity when there is no current running through it in the open circuit condition.

By putting I = 0 in equation **(1)** [22], The Voc may be derived

$$V_{oc}=(nkT/q)\ \mathrm{Ln}\left[(I_L/I_0)+1\right] \quad (2)$$

As demonstrated in [23], the fill factor FF may be ascertained empirically. Usually, it is expressed as a percentage (%).

$$FF = P_{max}/ V_{oc}*I_{sc} \quad (3)$$

Here P_{max} is the maximum power output of the solar panels.

The perpendicularity of the curve of the dependence of the current on the solar electricity cells voltage is indicated by the fill factor. The solar cell performs better when the I-V curve is squarer-more shaped. In general terms, it denotes the solar cell's maximum power extraction capacity relative to its optimum power [24]. The concept of efficiency is the most frequently employed metric to compare the results of various solar cells.

The percentage of incident power adapted to electrical power is the measure of a direct sunlight cell's productivity (η) [25].

$$\eta=(V_{oc} * I_{sc} * FF * 100 / P_{in} *S) \quad (4)$$

where P_{in} is the incident power of the sun ((in W/m², often 1000 W/m² under STC Standard Test Conditions), **S** in m^2 is the cell area, and I_{sc} is the short circuit current.

3. Results and discussion

Figs. 3 and 4 present the current-voltage (I-V) and power-voltage (P-V) properties of the GaAs(n)/GaAs(p) reference cell using the simulation results from Silvaco. First, we explore the influence of the n-type film thickness (The enriched layer's thickness, n ranges from 0.05 to 0.3 µm), while the doping concentration was set at $1\times10^{18}\ cm^{-3}$ and $1\times10^{19}\ cm^{-3}$ for n-type and p- type regions, respectively, and the deposition thickness of the p-type layer was set at 5 µm.

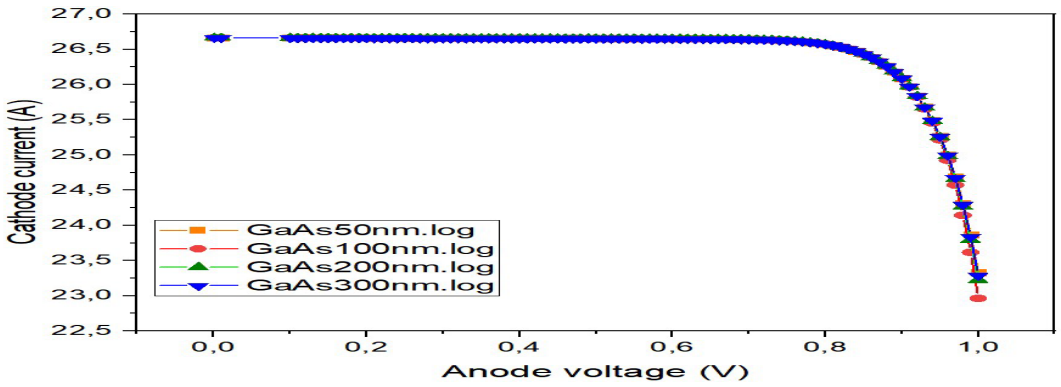

Fig. 3. Electrical characteristic current-voltage of GaAs (n) /GaAs (p) solar cell with constant p-GaAs thickness (5 µm) and variable n-GaAs thickness.

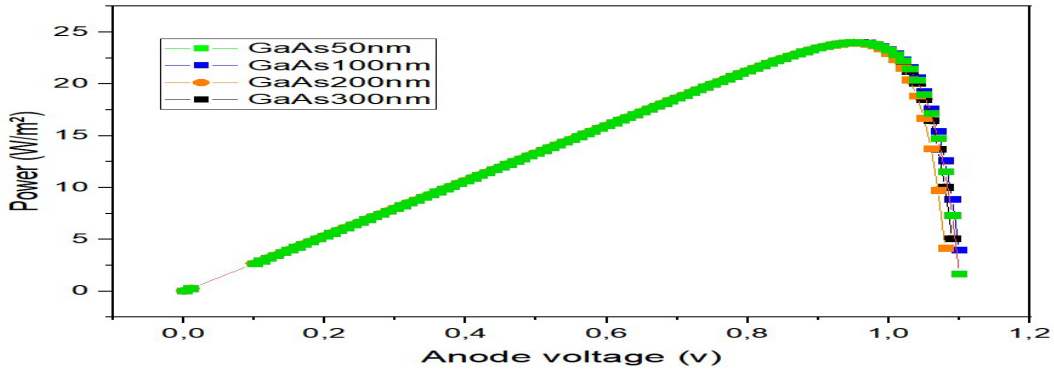

Fig. 4. Power dependence of a GaAs (n)/GaAs (p) solar cell with variable n-GaAs thickness and constant p-GaAs thickness (5 µm) on voltage P(V).

The obtained data suggest that the dimension of the n-type doped GaAs region has little effect. Therefore, we use a thicker GaAs of 0.1 µm. Next, figs. 5 and 6 depict the current-voltage and power-voltage curves for varying p-GaAs layer thicknesses (D_{GaAs} ranges from 0.5 to 6 µm), respectively, to draw attention to the effect of the layer's thickness. These outcomes are attained by keeping the n-GaAs layer thickness constant at 0.1 µm. When adding a new p-type layer, the most crucial part is figuring out how thick it should be. The yield (η), open-circuit voltage (V_{oc}), and short-circuit current density (J_{sc}) must all be calculated in relation to the top cell's raised base thickness.

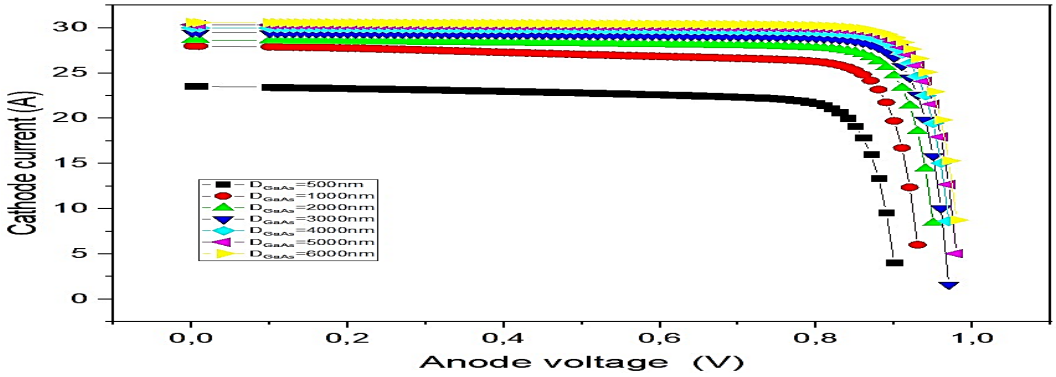

Fig. 5. Current-voltage dependence of a GaAs (n)/GaAs (p) solar energy device in variable p-GaAs thickness and a constant n-GaAs thickness of 0.1 µm.

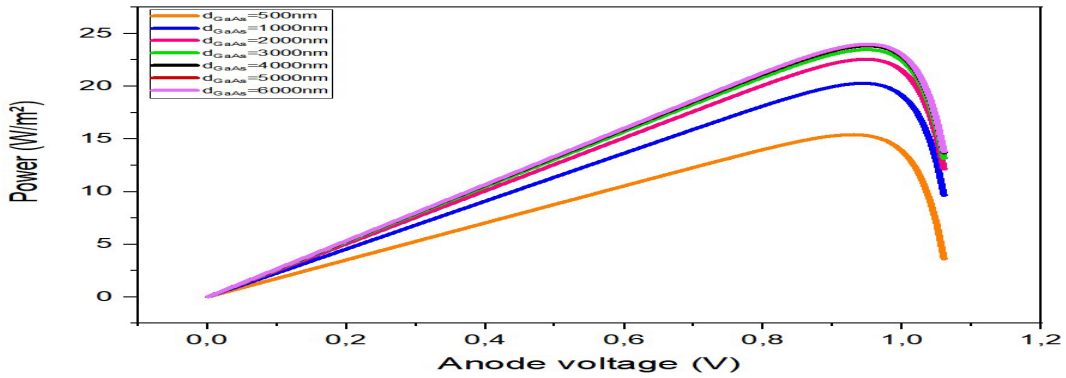

Fig. 6. Power dependence on the voltage of GaAs (n)/GaAs (p) solar cells with constant n-GaAs thickness (0.1 µm) and varying p-GaAs thickness.

It is evident from Figs. 5, 6, and 7 that the values of V_{oc}, J_{sc}, FF, and η rose in direct proportion to the p-GaAs layer's thickness. Fig. 7b displays the maximum power, which is 23.998 mW/cm^2. However, above 5 µm, these features attained their maximum values. In general, the carrier transfer length needs to be greater than the base thickness when designing solar cells. Before recombination, the photovoltaic cell p-n junction separates the carrier molecules produced by light [26]. Since doping is a physical parameter that affects a pn junction's performance and defines a semiconductor's conductivity, we first fixed the structure's parameters and then vary the level of doping between regions n and p, which affected the current that the structure provides. These features, shown in Table 2, revealed that when the doping dose rose above 1×10^{18} cm^{-3} (with the type P doping level at 1×10^{19} cm^{-3}), it increased, and the structure's morphology may deteriorate [27].

Table 2. Cell characteristics as a function of Nd emitter doping.

Transmitter doping Nd (cm^{-3})	**J_{sc} (mA/cm²)**	**V_{oc} (V)**	**FF (%)**	**η (%)**
1×10^{16}	26.622	0.883	86.020	20.2
1×10^{17}	26.627	0.981	85.247	22.3
1×10^{18}	26.661	1.085	82.773	23.9
5×10^{18}	26.721	1.179	87.594	27.6

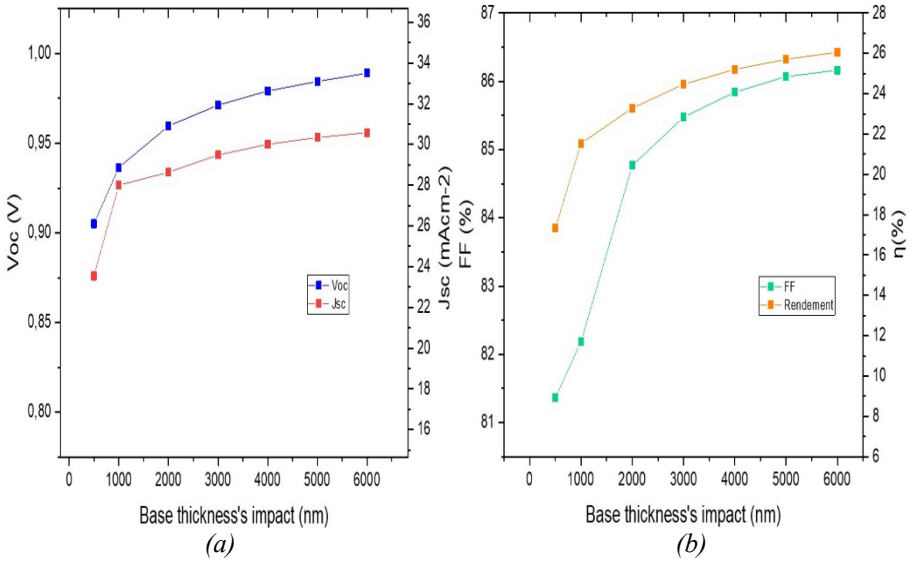

Fig. 7. (a) Variation of V_{oc} and J_{sc} depending on the thickness of the p-GaAs region, (b) Fill factor and η fluctuations based on p-GaAs level thickness.

The same logic was applied to the p area, based on Na, while keeping the doping level in the n region at $1\times10^{18}\,cm^{-3}$. Fig. 8 displays the resultant current-voltage curve, which demonstrates that the strongest current increased with the concentration of doping shifts. As excessive doping lowers current and consequently carrier mobility, we suggest gently doping the p area to achieve a maximum current [28,29]. Therefore, doping concentration is a parameter that affects the structure's performance, nevertheless, in order to prevent the possibility of a Schottky contact, critical levels must not be exceeded [30]. As a conclusion, $1\times10^{15}cm^{-3}$ was chosen to dope region p and 1×10^{18} cm^{-3} to dope region n.

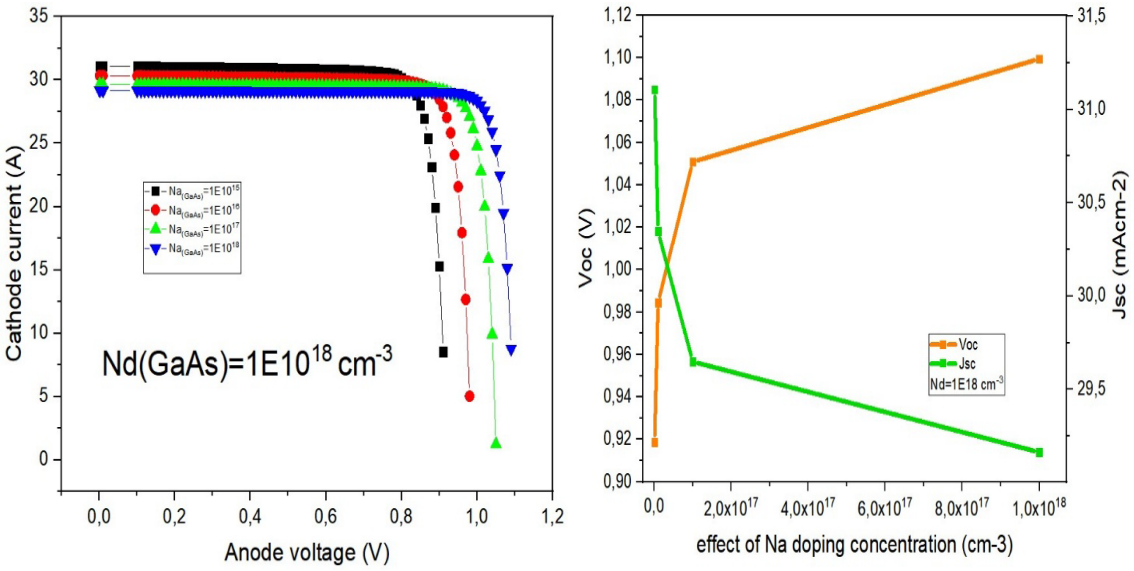

Fig. 8. (a) Current dependence on GaAs(p)/GaAs(n) homojunction cell voltage by varying the doping concentration of the Nd donor level, (b) Influence of varying GaAs region doping concentration on cell performance.

With the same input parameters already recorded in Table 1, a preliminary study conducted on Silvaco allowed us to simulate the two structures GaAs-p/GaAs-n and $B_xGa_{(1-x)}$ As-p/GaAs-n (x=1.46%) and to examine the effects of the geometric and physical attributes of the GaAs(p)/GaAs(n) homojunction cell to determine the most efficient parameters. According to the data in Table 3 and with the help of literature [31], a homojunction cell outperforms a heterojunction cell in terms of efficiency. The GaAs-p/BGaAs-n heterojunction structure optimized following this simple comparison. The simulated values of Voc (0.893 V) and Jsc (30.999 mA/cm²) are consistent with previously reported values for III-V material-based devices [32]. This finding serves to substantiate the reliability of the model. Subsequent experimental endeavors are scheduled to produce analogous structures and provide direct validation of these findings.

Table 3. Output parameters of structure pn.

Solar cells	V_{oc} (V)	J_{sc} (mA/cm²)	FF (%)	η (%)
GaAs(p)/GaAs(n)	0.893	30.999	81.245	22.5
$B_xGa_{(1-x)}$ As(p)/GaAs(n)	0.716	32.493	84.302	19.6

The electrical characteristics of current-voltage and power-voltage are illustrated in Fig. 9. According to Fig. 9b the GaAs(n)/GaAs(p) homojunction cell's maximum power P_{max} is 22.497 mW/m². In order to guarantee maximum photogeneration, a PIN structure was simulated, which is more efficient than a PN structure [33].

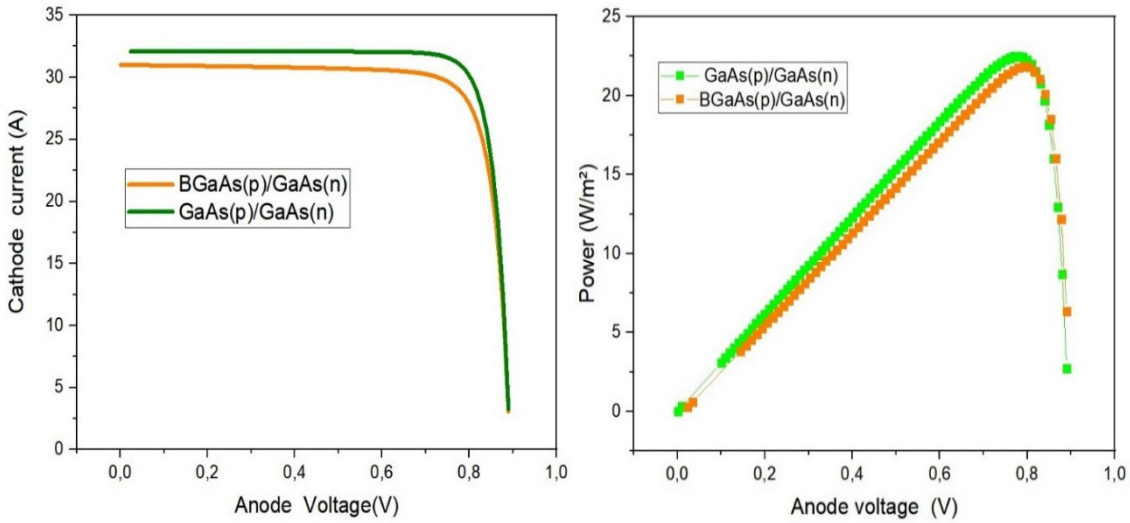

Fig. 9. (a) the variation of current as a function of the voltage for the GaAs(p)/GaAs(n) cell and the BGaAs(p)/GaAs(n) cell, (b) power variation as a function of the voltage for the GaAs(p)/GaAs(n) cell and the BGaAs(p)/GaAs(n) cell.

Therefore, in this context we developed our study by improving a conception or "design" most widely used in field solar cells. GaAs-based PIN solar cells have a distinctive set of advantages, including high efficiency, wide spectrum response, low-light performance, durability, and stability. These attributes make solar cells perfect for a variety of applications requiring specialized and demanding solar products. The p- layer is crucial to the distribution of the electronic field [33], since it only slightly interferes with the absorption of the sun's radiation spectra, necessitating the addition of a p+ layer in a new configuration (see Fig. 2). In fact, a structure's layer graduation helps to raise both its fill factor (FF) and yield (η). Furthermore, significant doping of the p layer (emitter) results

in electron-hole pairs, which encourage light to enter the intrinsic area and boost efficiency (see Table 4) [34].

Table 4. Output parameters based on P⁺PIN and PIN structure: GaAs/BGaAs/GaAs.

Solar cells	V_{oc} (V)	J_{sc} (mA/cm²)	FF (%)	η (%)
PIN (GaAs.p/BGaAs.i/GaAs.n)	1.034	27.527	88.534	25.2
*P⁺PIN (*GaAs.p⁺*/GaAs.p/BGaAs.i/GaAs.n)*	1.038	30.759	88.509	28.3

As a result, the P⁺PIN structure showed an improvement in the FF and η quality because a thin window layer was deposited above the P layer, which maximized photon absorption and increased the formation of photo-carriers [35,30]. Stated differently, enhancing the window layer's doping results in a decrease in the potential barrier and an increase in Z.C.E., which in turn enhances the collection of photo-generated carriers (see Table 4 and Fig. 10).

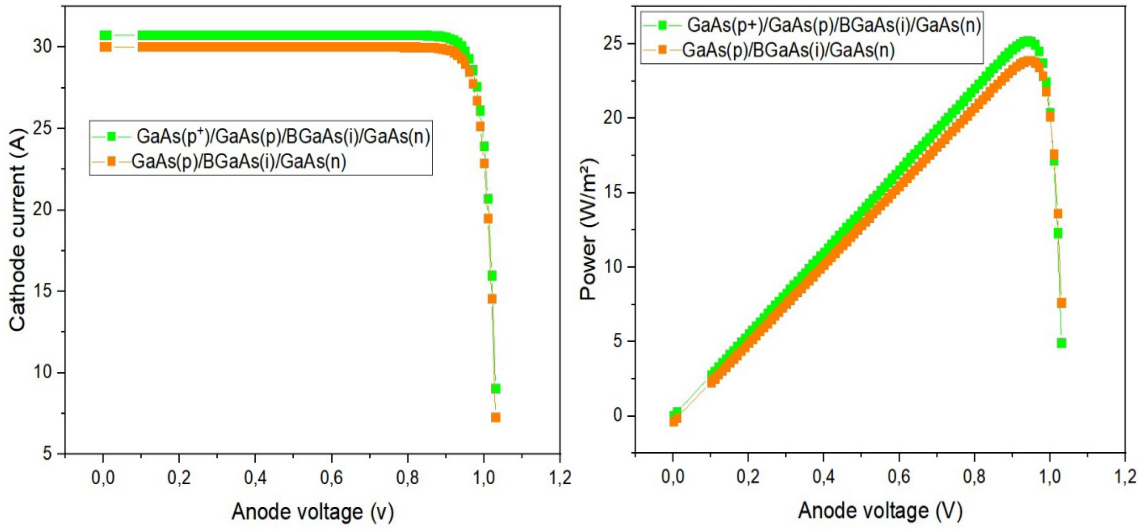

Fig. 10. (a) Current dependence on voltage for both PIN and P+PIN structures, (b) power evaluation as a function of the voltage of PIN and P+PIN cells.

Table 5 demonstrates that the outcomes of our study are on par with those of other III-V based solar cells. In this test simulation, the P⁺PIN test's structure has a yield of about 28%.

Table 5. Solar cell conversion efficiency values for different III-V semiconductor structures.

Solar cell	yields	reference
PIN (GaAs/BGaAs/GaAs)	25.2%	This work
P^+PIN(GaAs/GaAs/BGaAs/GaAs)	28.3%	This work
InGaP/GaAs	*26.9*%	[36]
GaAlAs(p)/GaAs(n)	25.8%	[37]
$In_{0.5}$ $Ga_{0.5}$ P(n)/GaAs(p)	15.5-16.3%	[38]
InGaN PN junction	26.6%	[32]
single GaAs solar	29.7%	[6]
Single -junction III-V	25.4%	[39]
Single -junction GaAs	19.7%	[40]
PIN InGaAs Solar Cell	33.7%	[41]

4. Conclusions

The efficacy and rapidity of the multi-junction photovoltaic cell structure have been successfully developed through modeling and simulation. By discovering the "perfect" solution for doping levels and layer thickness, artificial intelligence can assist in searching the large solution space for the ideal specifications for high-efficiency solar electricity cells. On the other hand, PN, PIN, and P^+PIN solar cells are created, modeled, and refined. The most efficient materials and parameters must be chosen because the "active layer" is an essential structural component of cell design. As a result, altering the emitter's thickness improved efficiency. Next, both the thickness and doping of the base are important considerations. Plotting and extracting simulation data, such as current-voltage and power-voltage characteristics, were performed. To find the most efficient combination of the three cells, a thorough simulation analysis was conducted. A comparison was made between the V_{oc}, J_{sc}, FF, and efficiency of PN, PIN, and P^+PIN solar cells. We have achieved a 3% improvement over the simple PIN structure.

Therefore, we can validate that the BGaAs layer has a good response in the solar cell module. Moreover, when exposed to sunlight with an AM1.5G spectrum, the P^+PIN solar cell exhibited the greatest capacity for conversion, reaching up to 28.3%. In conclusion, the advancement of economical, high-performance solar cells and layers must continue so as to open up opportunities.

References

[1] Li, J., et al., Frontiers in Physics 8 (2021): 631925; https://doi.org/10.3389/fphy.2020.631925

[2] Nelson, Jenny A., The physics of solar cells, World Scientific Publishing Company, 2003; https://doi.org/10.1142/p276

[3] Wang, Shuang, et al., Energy Materials 5.8 (2025): N-A; https://doi.org/10.20517/energymater.2024.303

[4] Li, Q., et al., Europhysics Letters 71.6 (2005): 994; https://doi.org/10.1209/epl/i2005-10170-7

[5] Hossain, Md Faruk, Shuhei Yagi, Hiroyuki Yaguchi, AIP Advances 15.2 (2025); https://doi.org/10.1063/5.0247676

[6] Nikolić, Veljko, Nebojša Janković, Proceedings of Small Systems Simulation Symposium, Niš, Serbia. 2012.

[7] Attari, K., Amhaimar, L., Asselman, A., Bassou, M., International Journal of Photoenergy, 2017; https://doi.org/10.1155/2017/8269358

[8] Manual, ATLAS User'S, Device simulation software, Silvaco Int., Santa Clara, CA (2008).

[9] Atlas User's Manual Device Simulation Software; Silvaco, Inc. 4701 Patrick Henry Drive, Bldg. 2 Santa Clara, CA 95054 October 2, 2013.

[10] Khelifi, Samira, Abderrahmane Belghachi, Revue des Energies Renouvelables 7.1 (2004): 13-21; https://doi.org/10.54966/jreen.v7i1.861

[11] Silvaco, I., ATLAS User's Manual: Device Simulation Software; Silvaco Int., Santa Clara, CA, USA 2019 (2018).

[12] Ilahi, Soufiene, et al., Physica B: Condensed Matter 421 (2013): 105-109; https://doi.org/10.1016/j.physb.2013.03.045

[13] Yan, Yingce, Yanlong Wang, Huifang Ma, Chinese Journal of Computational Physics 33.2 (2016): 221.

[14] Kharchich, Fatima Zahra, Abdellatif Khamlichi, Optik 272 (2023): 170196; https://doi.org/10.1016/j.ijleo.2022.170196

[15] Manual, ATLAS User'S, ATLAS User's Manual: Device Simulation Software, Version 5.15. 32. R. R, Santa Clara, CA, USA (2010).

[16] Sahoo, G. S., G. P. Mishra, Superlattices and Microstructures 109 (2017): 794-804; https://doi.org/10.1016/j.spmi.2017.06.002

[17] Lindsay, A., E. P. O'Reilly, Physica Status Solidi C 5.2 (2008): 454-459; https://doi.org/10.1002/pssc.200777456

[18] Hamila, R., et al., Journal of luminescence 129.9 (2009): 1010-1014; https://doi.org/10.1016/j.jlumin.2009.04.013

[19] Sander, Thomas, et al., Physical Review B-Condensed Matter and Materials Physics 83.23 (2011): 235213; https://doi.org/10.1103/PhysRevB.83.235213

[20] Sharma, Arvind, Journal of Electronic Materials 49 (2020): 6263-6269; https://doi.org/10.1007/s11664-020-08389-z

[21] Lindholm, Fredrick A., Jerry G. Fossum, Edward L. Burgess, IEEE transactions on electron devices 26.3 (2005): 165-171; https://doi.org/10.1109/T-ED.1979.19400

[22] Singh, Khomdram Jolson, Subir Kumar Sarkar, Optical and Quantum Electronics 43 (2012): 1-21; https://doi.org/10.1007/s11082-011-9499-y

[23] Zidani, Ikram, et al., East European Journal of Physics 1 (2025): 141-150; https://doi.org/10.26565/2312-4334-2025-1-13

[24] Solanki, Chetan Singh, Solar photovoltaics: fundamentals, technologies and applications, Phi learning pvt. Ltd., 2015.

[25] Saga, Tatsuo, Npg Asia Materials 2.3 (2010): 96-102; https://doi.org/10.1038/asiamat.2010.82

[26] Lounis, A., et al. TCAD simulations of ATLAS pixel guard ring and edge structure for SLHC upgrade. No. ATL-UPGRADE-PUB-2010-001. ATL-COM-UPGRADE-2009-013, 2010.

[27] Salem, Marwa S., et al., Semiconductor Science and Technology 34.3 (2019): 035012; https://doi.org/10.1088/1361-6641/ab0078

[28] Serdouk, Mohammed Ridha, Etude par simulation numérique des propriétés électriques d'une cellule solaire en silicium amorphe hydrogéné (a-Si: H). Diss. Université Mohamed Khider-Biskra, 2015.

[29] Mimoune, Mohamed, Étude des capteurs photovoltaïques basés sur les nanotechnologies, Diss. Université du Québec à Trois-Rivières, 2016.

[30] Mallem, Izzeddine, Simulation des cellules solaires hétérojonction Si-SiGe par SILVACO, Diss. Université Mohamed Khider-Biskra, 2014.

[31] El-Huni, Walid, Modélisation de cellules solaires multi-tandem bas coût et très haut rendement à base de nitrures des éléments III-V, Diss. Université Paris Saclay (COmUE), 2016.

[32] Mesrane, A., et al., International Journal of Photoenergy 2015.1 (2015): 594858; https://doi.org/10.1155/2015/594858

[33] Makambo, John Beya, Performance and Assessment of Tandem Galnp/GaAs dual-junction solar cells using SCAPS-1D, University of Johannesburg (South Africa), 2022.

[34] Hamady, Sidi Ould Saad, Simulation numérique et caractérisation de matériaux semi-conducteurs III-N pour détecteurs ultraviolet et cellules solaires, Diss. Université de lorraine, 2017.

[35] Khelifi, Samira, Abderrahmane Belghachi, Revue des Energies Renouvelables 7.1 (2004): 13-21; https://doi.org/10.54966/jreen.v7i1.861

[36] Mohamed, Esmeel T. et al., Sustainable Energy Technologies and Assessments 44 (2021): 101067; https://doi.org/10.1016/j.seta.2021.101067

[37] Abderrezek, M., et al., Elektronika ir Elektrotechnika 19.8 (2013): 41-44; https://doi.org/10.5755/j01.eee.19.8.5392

[38] Hwang, Sun-Tae, et al., Solar Energy Materials and Solar Cells 182 (2018): 348-353; https://doi.org/10.1016/j.solmat.2018.03.037

[39] Jomen, Ryota, et al., Japanese Journal of Applied Physics 57.8S3 (2018): 08RD12; https://doi.org/10.7567/JJAP.57.08RD12

[40] Al-Ezzi, Athil S. Ibrahim, M. N. M. Ansari, Journal of the Korean Physical Society 86.3 (2025): 245-262; https://doi.org/10.1007/s40042-024-01260-y

[41] Sahoo, Girija Shankar, Guru Prasad Mishra, IEEE Transactions on Electron Devices 66.1 (2018): 153-159; https://doi.org/10.1109/TED.2018.2859766